



Australian Government
Department of Defence
Defence Science and
Technology Organisation

Modelling and Experimental Validation of the Acoustic Electric Feedthrough Technique

Scott Moss, Phillip McMahon, Michael Konak, Chris Phoumsavanh, Nik Rajic,
Steve Galea, Ian Powlesland*

Air Vehicles Division
***Maritime Platforms Division**
Defence Science and Technology Organisation

DSTO-RR-0338

ABSTRACT

This report outlines an investigation of an ultrasonic Acoustic Electric Feedthrough (AEF) to transfer power through a metal plate. This approach is being explored as a potential means of wirelessly powering in situ structural health monitoring systems embedded within aircraft and other high value engineering assets. A numerical model is developed describing the coupled electro-mechanical behaviour of an AEF system, and is then validated using experimental data. Using a pair of well matched piezoelectric disks with 38 mm diameter and 2 mm thickness, and with 1 W of real input power, the AEF approach is shown to transfer approximately 300 mW of usable electrical power through aluminium plate with thicknesses in the range of 1.6 mm - 5 mm.

RELEASE LIMITATION

Approved for public release

Published by

*Air Vehicles Division
DSTO Defence Science and Technology Organisation
506 Lorimer St
Fishermans Bend, Victoria 3207 Australia*

Telephone: (03) 9626 7000

Fax: (03) 9626 7999

© Commonwealth of Australia 2008

AR-014-343

November 2008

APPROVED FOR PUBLIC RELEASE

Modelling and Experimental Validation of the Acoustic Electric Feedthrough Technique

Executive Summary

In-situ Structural Health Monitoring (SHM) devices allow the Australian Defence Force to move from expensive time-based maintenance approaches for ageing platforms to cost-effective condition-based approaches. For air platforms the retrofitting of these systems is complicated by the fact that the majority of SHM devices need to be fitted on internal aircraft structure, underneath the aircraft's skin. If the SHM device is in a location that is difficult to access, then transferring power and data through the aircraft skin may be necessary. The retrofitting of the SHM device then becomes complicated due to flight worthiness and certification issues, with the chief concern being that holes drilled through the aircraft skin (to pass wiring) could, for example, act as stress concentrators. To address this issue DSTO has investigated the use of an ultrasonic Acoustic Electric Feedthrough (AEF) technique to pass power and communications through metal plates. The AEF technique consists of generating, transmitting and receiving high frequency (kHz-MHz) acoustic pulses using piezoelectric elements. A numerical AEF modelling capability was developed, and used to explore the effect of: (i) metal plate thickness, (ii) piezoelectric element thickness, (iii) the type of piezoelectric material, and (iv) the bondline thickness between the piezoelectric element and metal plate. An experimental program was carried out to validate the model predictions. Experimental studies using a non-optimized system have shown that the AEF approach was able to transfer in the range of 300 mW of real electrical power (for 1000 mW of real input power) through aluminium plates with a thickness range of 1.6 mm – 5 mm, typical for aircraft skin. For comparison, a standard recharge on an 80 mA-hr lithium polymer battery requires four hours of charging at a power level of approximately 148 mW, indicating that the demonstrated 300 mW AEF power transfer would be more than sufficient to recharge a small battery.

Authors

Scott Moss

Air Vehicles Division

Scott Moss received a B.App.Sci. in Applied Physics in 1990 from the Royal Melbourne Institute of Technology, winning the Walter Boas Memorial Prize that year. He was a contract lecturer/tutor at RMIT during 1991-1992, studied towards a PhD at RMIT during 1993-1996 investigating electrical contacts to high temperature superconductors, was a Research Associate at the University of Wollongong in 1997 investigating Uranium doping of Bismuth HTS tapes, a Junior Lecturer at the University of Tasmania in 1998-1999 teaching physics and electronics. He completed his PhD in 1999, the same year he joined DSTO Air Vehicles Division to mainly work on the development of the 'smart patch' composite repair for the RAAF F/A-18. In 2003 he was awarded a Defence Science Fellowship and spent a year at UCLA investigating energy harvesting from aircraft structures. This work continues as an exploration of techniques for powering, and communicating with, structural health monitoring devices.

Phillip McMahon

Maritime Platforms Division

Phillip McMahon received a BSc in 1988 in Applied Physics from the Royal Melbourne Institute of Technology (RMIT). He completed a Ph.D at RMIT University in 1995. He then pursued an academic career at The University of Tasmania lecturing in Physics and Electronics between 1996 until 1998. He took up an Australian Postdoctoral Research Fellowship in The School of Physics at the University of Melbourne conducting research work on phase imaging of synchrotron and neutron radiations between 1998-2002. Then joined the DSTO in 2002 and has worked in Maritime Platforms Division conducting research into micro sensors for structural health monitoring and more recently applications of nanotechnology for Defence.

Michael Konak

Air Vehicles Division

Michael Konak has a Certificate of Technology in Electronics from the Royal Melbourne Institute of Technology (RMIT) 1980 and a B.Eng. (Hons.) in Electronic Engineering also from RMIT in 1989. He joined Structures Division at the Aeronautical Research Laboratory Melbourne in 1988. He has been involved in the design and implementation of instrumentation systems used for fatigue analysis of aircraft structures and contributed to research on a self-powered health monitoring system and vibration suppression using piezoelectric devices, related to aircraft structures. He is currently a Science and Technology Officer in the Air Vehicles Division at DSTO Melbourne.

Chris Phoumsavanh

Air Vehicles Division

Chris Phoumsavanh received the Vice Chancellor's Scholarship in Engineering at Swinburne University of Technology in 2005. He has a one year contract with DSTO Smart Structures and Advanced Diagnostics, where he is investigating Acoustic Electric Feedthrough communications and powering. Chris' time at DSTO is supported by the DSTO Industry Experience Program while he is working towards his Bachelor of Engineering (Robotics & Mechatronics) and Bachelor of Science (Computer Science & Software Engineering). In 2003 he was selected to attend the 32nd Professor Harry Messel International Science School, and in 2005 was invited to attend as a student staff member.

Nik Rajic

Air Vehicles Division

Nik Rajic received a B.Eng. (Hons.) in Mechanical Engineering from University of Melbourne in 1989. He joined Structures Division at the Aeronautical Research Laboratory in 1991 and in 1992 undertook studies at Monash University which led to the completion of a PhD in 1995. He has since contributed to research on fatigue-life extension techniques, thermoelastic stress analysis, thermoplasticity, thermographic nondestructive evaluation, and in situ structural health monitoring techniques based on smart structures principles. He is currently a Senior Research Scientist in the Air Vehicles Division.

Steve Galea
Air Vehicles Division

Dr Galea graduated in 1980 with a Bachelor of Engineering (Mech.) from the University of Queensland with first class honours and in 1983 he received a Masters of Engineering Science. He commenced employment with the Aeronautical Research Laboratory in 1983. In 1985 he commenced studies at the Institute of Sound and Vibration Research, University of Southampton, UK and received his Doctor of Philosophy from the University of Southampton in 1989. Dr Galea is currently a Principal Research Scientist and Functional Head of the Smart Structures and Advanced Diagnostics Group. His current responsibilities involve the management of research and providing technical leadership on the development and application of smart materials and structures technologies to aircraft structures, including in-situ structural health monitoring and self-powering techniques. He has an extensive publication record of over 80 publications, which include three book chapters on smart structures and repairs to acoustically-fatigued structures. Dr Galea is a member of the Editorial Board on the International Journal of Structural Health Monitoring and is the section editor of the Aerospace Applications section in the Encyclopaedia of Structural Health Monitoring. He is also on the Management Steering Committee for the DSTO Key Initiative on Smart Structures and Materials and on the Advisory Board of the ARC Centre for Complex Dynamic Systems and Control.

Ian Powlesland
Air Vehicles Division

Ian Powlesland joined the then Aeronautical Research Laboratories in 1972. Has predominantly worked with structural testing instrumentation since that time. This has included early dedicated portable signal averaging equipment, Nomad, CT4 and F18 fatigue test control systems and some field trials. Currently he is working in the field of autonomous damage and loading sensors for managing an aging fleet.

Contents

LIST OF FIGURES	II
NOMENCLATURE	IV
1. BACKGROUND.....	1
1.1 LTSpice Modelling of a Single Piezoelectric Disk.....	1
1.2 LTSpice Modelling of the Acoustic Electric Feedthrough.....	4
1.3 Range of Validity of LTSpice Modelling.....	6
2. EXPERIMENTAL	8
3. RESULTS AND DISCUSSION	12
3.1 Part 1 - Steel plate Acoustic Electric Feedthrough.....	12
3.2 Part 2 - Aluminium plate Acoustic Electric Feedthrough.....	16
4. CONCLUSION	23
5. REFERENCES	24
APPENDIX A: EXAMPLE PIEZO PARAMETER CALCULATION	27
APPENDIX B: LTSPICE NETLISTS	29
B.1. PZTtrans.lib.....	29
B.2. PZTtrans.asy.....	29
B.3. const_power.lib.....	30
APPENDIX C: PARAMETER VALUES USED IN CALCULATIONS	31

List of Figures

Figure 1: (a) Schematic of a piezoelectric disk in air and (b) the equivalent LTSpice model.	2
Figure 2: Admittance spectrum measured for a Pz27 disk with 38 mm diameter and 2 mm thickness showing the thickness resonant mode T and the coupled radial modes R [21].	3
Figure 3: Schematic showing an AEF configuration in cross-section.	4
Figure 4: LTSpice model of a Pz27/steel AEF system with similar physical configuration to that shown in Figure 3, being the AEF geometry discussed in the literature [9, 10].	5
Figure 5: LTSpice schematic of a Pz27/Al AEF system with similar physical configuration to that shown in Figure 3 and with constant 1 W apparent input power and diode bridge RC load.	5
Figure 6: Schematic of the constant power source.	6
Figure 7: Attenuation caused by diffraction, after Johansson [27] and Kino [28].	7
Figure 8: Schematic of the AEF power transfer experimental arrangements for (a) steel plate (b) aluminium plate.	9
Figure 9: Impedance measurements using (a) Solartron 1260 and (b) the DSTO piezoelectric disk adaptor.	11
Figure 10: Pz27 element immediately after silver-epoxy bonding to aluminium plate.	11
Figure 11: Simulation results comparing (a) the voltage ratios and (b) the admittance for three cases: (i) literature reproduced from Hu et al [9], (ii) LTSpice modelling using lossy transmission line damping models for the piezoelectric and steel elements and (iii) the LTSpice model with 100 μm silver epoxy bondlines added between the piezoelectric elements and the steel.	12
Figure 12: Measured impedance magnitude spectrum over the frequency range 1 kHz-10 MHz, and modelled data in the vicinity of the fundamental through-thickness resonance (~972 kHz).	13
Figure 13: Comparison of measured and modelled (a) impedance magnitude and (b) phase near the thickness resonance, where thickness mode resonance has been labelled with T and the radial coupled modes are labelled R.	14
Figure 14: Oscilloscope screen capture showing three traces from steel plate AEF experiment. Channel locations are indicated in Figure 8a: Ch1=V(in), Ch2=I(R2), Ch3=V(out) across 20 Ω .	14
Figure 15: Measured versus modelled power transfer efficiency for a 1 mm Pz27/6 mm steel/2 mm Pz27 AEF system. Note the peaky nature of the plot with very low power transfer between the peaks.	15

Figure 16: Impedance measurements of 2 mm thick Pz27 disks before and after bonding to 1.6 mm Al plate: (a) shows the measured impedance magnitude from the transmit piezoelectric element, for both transmit and receive piezoelectric elements (b) shows details of the measured impedance magnitude near the fundamental thickness resonance and (c) the corresponding phase..... 17

Figure 17: Oscilloscope screen capture showing four example voltage traces from the aluminium plate AEF experiment. Channel locations are indicated in Figure 8b: Ch1=V(in), Ch2=I(R2), Ch3=V(out) across 30 Ω , Ch4=voltage across the receive piezo..... 18

Figure 18: Measured and modelled results for the 2 mm Pz27/1.6 mm Al/2 mm Pz27 AEF configuration (a) load voltage and (b) transmitted power as a function of frequency. 19

Figure 19: Phase spectra for a 2 mm Pz27/1.6 mm Al/2 mm Pz27 AEF configuration..... 19

Figure 20: Measured and modelled results for the 2 mm Pz27/5 mm Al/2 mm Pz27 AEF configuration, (a) load voltage and (b) transmitted power as a function of frequency. 20

Figure 21: Modelled results for an AEF system with varying plate thickness and drive frequency using a 1 W constant apparent input power and a 30 Ω load resistor. 20

Figure 22: Modelled results for an AEF system for a 1.6 mm thick Al plate, where the PZT element thickness is varied: (a) 90% of steady state load voltage, (b) time taken to reach 90% of steady state load voltage, and (c) load power as a function of varying Pz27 thickness..... 21

Figure 23: Modelled results for 2 mm Pz27/1.6 mm Al/2 mm Pz27 AEF configuration, (a) load voltage and (b) load power, with varying load resistance and drive frequency swept across the fundamental thickness resonance, 1025-1150 kHz. 22

Nomenclature

$\epsilon_{33,r}^T$	unclamped relative dielectric constant (dimensionless)
ϵ_{33}^S	clamped dielectric constant (F/m)
ϵ_0	permittivity of free space, $\sim 8.8542 \times 10^{-12}$ (F/m)
e_{33}	piezoelectric constant (C/m ²)
k_T, k_P, k_{33}	electromechanical coupling constants (dimensionless)
d_{31}, d_{33}	piezoelectric strain constant in the 1 and 3 directions respectively (C/N)
Y_{33}^E	Young's modulus at constant field (N/m ²)
c_{13}^E	closed circuit elastic stiffness, i.e. electrodes shorted (N/m ²)
c_{33}^E	closed circuit elastic stiffness, (N/m ²)
c_{33}^D	open circuit elastic stiffness (N/m ²)
$s_{13}^E, s_{33}^E, s_{11}^E$ and s_{12}^E	closed circuit elastic compliances at constant E field (m ² /N)
v_D	clamped speed of sound (m/s)
Q	mechanical Q (dimensionless)
ρ	density (kg/m ³)
H	thickness of a PZT element (m)
R	radius of a PZT element (m)
A_E	area of a PZT element (m ²)
G	aspect ratio, height to radius, of a piezoelectric element
f_{AR}	anti-resonant frequency (Hz)
f_R	resonant frequency (Hz)
AEF	Acoustic Electric Feedthrough
PZT	Lead Zirconate Titanate

1. Background

The Australian Defence Science and Technology Organization (DSTO) is developing in situ structural health monitoring systems [1, 2, 3, 4, 5, 6, 7, 8] for potential use in high value platforms across the Australian Defence Force (ADF). Using smart sensor concepts, airframe damage and damage growth, operational strains, corrosion, corrosive environments, and other structural and environmental parameters, would be continuously monitored on-board an aircraft to provide a basis for real-time damage diagnostics. This technology could potentially permit a safe reduction in inspection and regular maintenance time and costs and therefore substantially impact on aircraft through-life support costs and availability. However providing power and two way communications to a smart sensor system is a challenge particularly when physical access to the system is difficult. To address this issue, DSTO is investigating the use of ultrasound via an Acoustic Electric Feedthrough (AEF) arrangement to provide power and communications through the skin of an aircraft to smart sensor systems located inside the aircraft.

Hu *et al* [9] modelled an AEF scheme from first principles. Sherrit *et al* [10] at the NASA Jet Propulsion Laboratory used lumped element modelling to reproduce Hu's work, and to extend the modelling of the AEF arrangement by adding a more realistic description of material damping. The AEF model implemented by Hu *et al* [9] and Sherrit *et al* [10] consisted of a metal plate sandwiched between two piezoelectric layers. Sherrit *et al* [10] highlighted the fact that their modelling did not incorporate adhesive bondlines between the piezoelectric material and the metal plate, the implicit suggestion being that the bondlines might affect the behaviour of an AEF system. This report examines the modelling of an AEF system in LTSpice, a complete and fully functional SPICE program from Linear Technology [11]. Implementing the model in LTSpice allows the complexity of the AEF modelling to be substantially increased by allowing: (i) the addition of extra AEF layers (i.e. bondlines) and (ii) the addition of realistic electrical components to the model. Once developed, the LTSpice AEF model was used to examine various geometrical and material parameters with the aim of optimizing the power transferred through a thin metal plate. To test the fidelity of the LTSpice modelling the simulations were compared to experimental data collected from AEF arrangements constructed to transfer power through both 1.6 mm and 5 mm thick aluminium plate.

1.1 LTSpice Modelling of a Single Piezoelectric Disk

Prior to modelling an AEF scheme it was necessary to ensure that LTSpice was capable of modelling the electromechanical behaviour of a single piezoelectric disk. There are numerous examples of lumped element and spice modelling of piezoelectric elements available in the literature [e.g. 10, 12, 13, 14, 15, 16]. Typically these are based on either the Mason [17] or the Krimholtz, Leedom and Matthaei (KLM) piezoelectric models [18]. Both the Mason and KLM piezoelectric models are one-dimensional and describe the thickness mode resonances of a piezoelectric element, utilizing a lumped element electrical circuit analog to model the electromechanical behaviour of the element.

The LTSpice modelling of a Lead Zirconate Titanate (PZT) element, as described in this paper, requires five piezoelectric material parameters: ϵ_{33}^S , e_{33} , c_{33}^D , ρ and Q . Some calculation may be required to implement a particular material type within LTSpice since PZT manufacturers rarely specify all of the required material parameters. The physical parameters used in these models vary depending on whether the piezoelectric element is *free* or *clamped*. An example of a free element is one hanging freely in air. Two examples given in the literature of clamped elements are: (i) a PZT element bonded to a 6 mm thick steel plate [10] and (ii) a PZT element bonded to a Poly Methyl Methacrylate (PMMA) acoustic load matching element [15]. The parameters are also dependent on geometry. Kim *et al* [19] used the aspect ratio G to investigate the effect of different piezoelectric disk geometries: e.g. a *pancake* defined by $G \ll 1$, and *cylinder* defined by $G \gg 1$. Often, key parameters like ϵ_{33}^S , e_{33} , and c_{33}^D will need to be calculated from other given piezoelectric material parameters. A series of equations that show how to calculate these particular parameters are given in Appendix A. These equations draw heavily on the various piezoelectric relationships highlighted by Berlincourt *et al* [20].

The LTSpice model of a PZT element shown in Figure 1 was adapted from the literature [10-16] and has three ports: two mechanical ports corresponding to the back (B) and front (F) of the element, and a single electrical port (E) with the assumption that the opposite side of the PZT element is grounded. PZT element mechanical losses are modelled using a *lossy transmission line* as outlined in the literature [14, 15]. The LTSpice library and schematic files for the model shown in Figure 1b are given in Appendix B, with parameter definitions given in Appendix C.

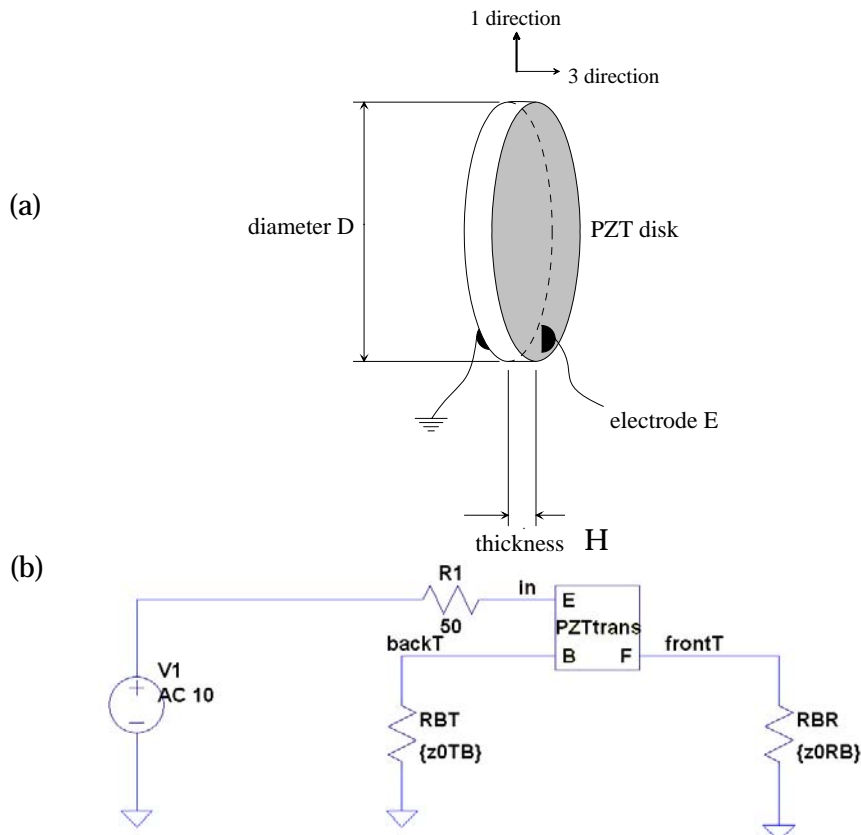


Figure 1: (a) Schematic of a piezoelectric disk in air and (b) the equivalent LTSpice model

Figure 1a shows a schematic of a piezoelectric disk element of diameter D and thickness H where the resistors RBT and RBR model the acoustic energy lost to the surrounding air. R1 is equal to 50Ω which is the typical output impedance of an AC voltage source. Most results presented in this paper, measured and modelled, were produced using piezoelectric elements with nominal dimensions of $D = 38 \text{ mm}$ and $H = 2 \text{ mm}$. According to Kim *et al* [19], for PZT-5, if the aspect ratio $G \sim 0.1$ there should be little or no mode coupling between the radial and thickness vibration modes and the electromechanical coupling constant used should be that for a pancake geometry, i.e. $k_T \sim 0.47$ [20]. The PZT disks used in the current work had an aspect ratio of approximately 0.1, yet a measured [21] impedance spectrum (Figure 2) revealed substantial mode coupling between the thickness and radial modes, marked T and R respectively. The observed mode coupling effect will be discussed later.

The PZT elements used in this paper were of a material composition denoted Pz27 [22], which is a ceramic with material properties similar to PZT-5A. The modelling results presented in this paper were calculated using a Pz27 electromechanical coupling constant of $k_{33} = 0.699$, where the 33 subscript denotes a cylindrical geometry. Interestingly, modelling the element using a pancake geometry (with $k_T \sim 0.47$) produced a substantially poorer fit to the measured data. It is worth noting that measured values of modelling parameters were used where possible. A list of parameters used for the piezoelectric calculations is given in Appendix C.

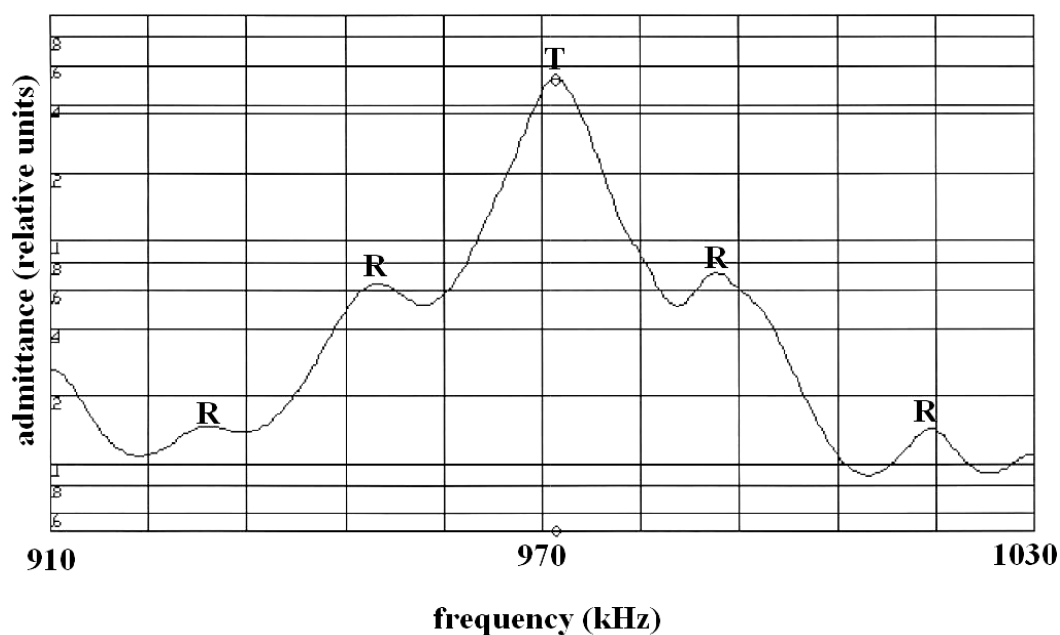


Figure 2: Admittance spectrum measured for a Pz27 disk with 38 mm diameter and 2 mm thickness showing the thickness resonant mode T and the coupled radial modes R [21]

1.2 LTSpice Modelling of the Acoustic Electric Feedthrough Technique

As mentioned, using LTSpice allowed the fidelity of the AEF modelling to be substantially increased over that presented in the literature by allowing: (i) the addition of extra AEF layers (i.e. bondlines) and (ii) the addition of realistic electrical components in the model. Figure 3 is a schematic cross-section of an AEF system showing the transmit and receive PZT elements bonded either side of a metal plate. Figure 4 and 5 show schematics of two AEF models that were implemented in LTSpice. Figure 4 depicts the model developed to extend the work of Hu *et al* [9] and Sherrit *et al* [10]. Figure 5 shows a schematic of the LTSpice model developed to examine acoustic energy transfer through an aluminium plate, and included the addition of a non-linear electrical load on the receive side of the model. Inclusion of realistic bondline thicknesses (i.e. shown as the components *LossyBondTline* in Figure 4 and 5) into the modelling was required to achieve reasonable correlation with measured AEF power transfer results, which will be discussed later in this report.

To perform a simulated frequency sweep with LTSpice a script was written to execute the following simple algorithm:

- modify the relevant parameter in the LTSpice netlist (e.g. frequency, plate thickness, piezo thickness),
- call LTSpice to perform a transient analysis,
- read the specified LTSpice measurements from the LTSpice log file,
- record the measured data,
- repeat until last frequency.

A simulated frequency sweep over the range 600 kHz -1300 kHz with 5 kHz steps would typically take 24 hours on a 3 GHz Pentium 4 duo-core machine with 3 Gb of fast RAM.

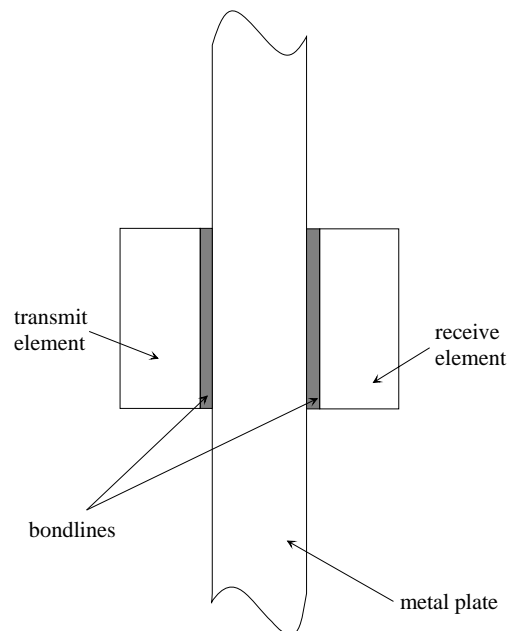


Figure 3: Schematic showing an AEF configuration in cross-section

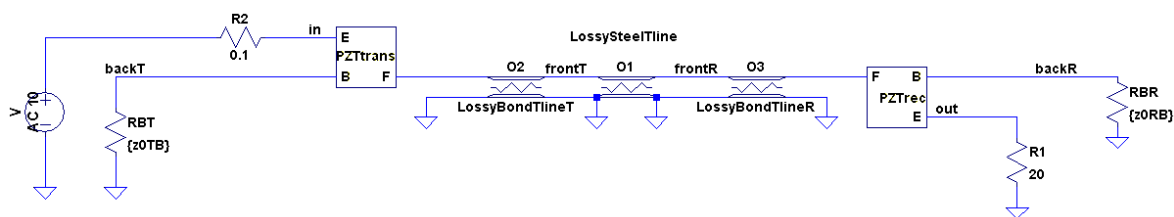


Figure 4: LTSpice model of a Pz27/steel AEF system with similar physical configuration to that shown in Figure 3, being the AEF geometry discussed in the literature [9, 10]

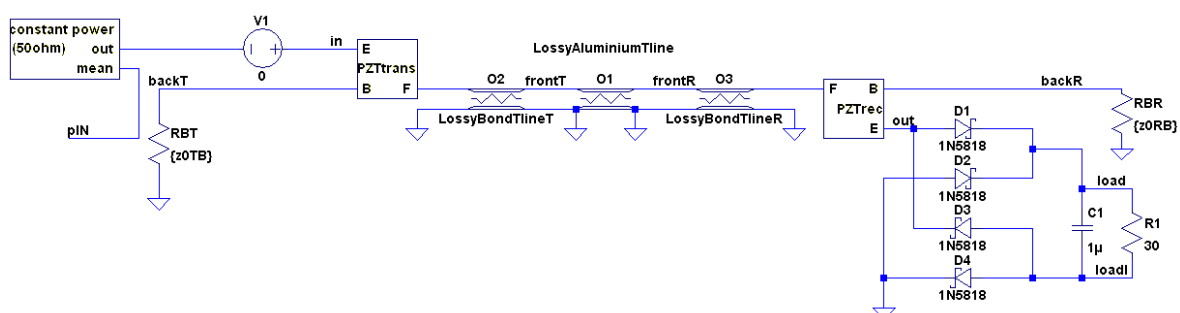


Figure 5: LTSpice schematic of a Pz27/Al AEF system with similar physical configuration to that shown in Figure 3 and with constant 1 W apparent input power and diode bridge RC load

Several factors were found to have an important influence on the power transfer efficiency of the AEF system, listed below:

(i) *Adhesive bondline*. As mentioned earlier, Sherrit *et al* [10] stated that the adhesive bondline between the piezoelectric element and the metal plate might limit the power transfer efficiency of an AEF system. In this report AEF systems with nominal bondline thickness of 100 μm were investigated using the LTSpice models shown in Figure 4 and 5. The bondlines are assumed to be silver loaded epoxy [23] with material properties given by Rajic [24].

(ii) *Supply impedance*. When using LTSpice to reproduce the steel plate case reported in the literature [9, 10] it was assumed that the supply output impedance was negligible (wire resistance only, which was modelled with $R2 = 0.1 \Omega$ as shown in Figure 4). The power amplifier utilised experimentally had an output impedance of 50 Ω and therefore modelling the aluminium plate AEF system required $R2 = 50 \Omega$ (Figure 5).

(iii) *Constant power source*. The schematic of the constant power source in Figure 5 is shown in Figure 6 and the associated library file is included in Appendix B. The constant power source model was developed to allow direct comparison between experimental observations and model predictions.

Normally 1 W of apparent input power was chosen to drive the AEF systems because this could easily be supplied by the amplifier without risk of damage. When the drive frequency

coincided with an AEF system resonance the phase difference between the input current and voltage was near zero meaning that there was approximately 1 W of real input power at resonance. The apparent input power was measured by taking the RMS of the instantaneous product of the input current and the input voltage.

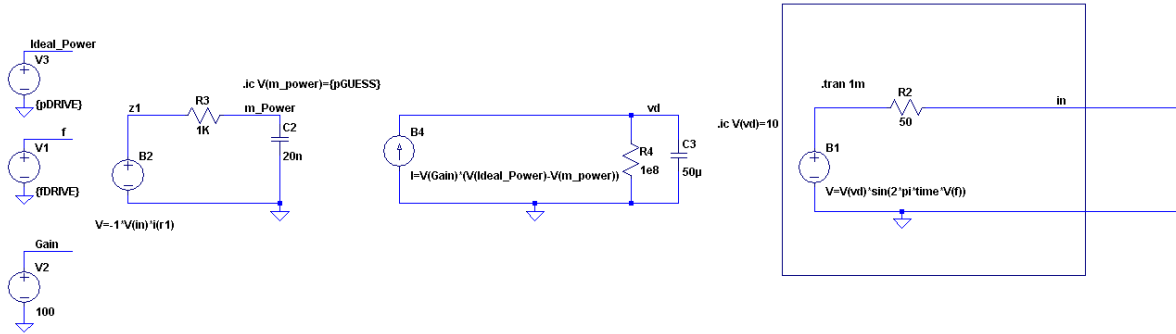


Figure 6: Schematic of the constant power source

(iv) *Material damping.* Damping in the piezoelectric elements is modelled using a lossy transmission line [14, 15]. The LTSpice models used in this report extend the use of the lossy transmission line to the metal plate and the bondlines.

(v) *Diodes.* High speed Schottky diodes were required to maximise the AEF power transfer efficiency. As shown in Figure 5, high speed 1N5818 diodes [25] were used to create the rectifying bridge on the receive side of the plate. The 1N5818 Spice model supplied by the manufacturer was modified to include measured values of diode leakage.

(vi) *Load resistance.* To duplicate the literature results the investigation of a steel plate AEF system required a linear 20 Ω load resistor as shown in Figure 4. A 30 Ω resistive load in parallel with a high frequency 1 μF storage capacitor was used for the investigation of aluminium plate AEF systems (R1 and C1 respectively in Figure 5). The reason for choosing a 30 Ω resistive load will be discussed later.

(vii) *Element thickness, $H = 2$ mm.* Pz27 disks with 38 mm diameter and 2 mm thickness were chosen for AEF investigations that involved aluminium plate. The 2 mm thickness was chosen because the fundamental anti-resonant frequency was approximately 1 MHz which was low enough to ensure that cable-inductance issues were negligible and, for demonstration purposes, simple drive electronics could be fabricated using commercially available MOSFET driver chips.

1.3 Range of Validity of LTSpice Modelling

The following section discusses various factors and restrictions on the accuracy of modelling an AEF system in LTSpice. It was expected that the 1-dimensional LTSpice models presented would produce useful predictions as long as the total acoustic path was less than the Fresnel distance for the solid i.e. the AEF system operated in the plane wave region. Mason [26] estimated that the Fresnel region extends for a distance,

$$d_0 \doteq \frac{R^2}{2\lambda} \quad (1)$$

For the AEF systems investigated in this paper, with a drive frequency of approximately 1 MHz and using a Pz27 disk with a diameter of 38 mm, equation 1 predicts a Fresnel distance of $d_0 \sim 90$ mm. Outside of the Fresnel region diffraction effects need to be included. Johansson and Martinsson [27] investigated the inclusion of diffraction effects in PSpice simulations of ultrasonic systems using an approximation of the equation given by Kino [28]. This describes the attenuation between two identical transducers with radius R and separated by distance x in terms of the Seki [29] parameter S ,

$$S = \frac{x\lambda}{R^2} \quad (2)$$

where λ is the wavelength of the ultrasound. It is assumed that equation 2 holds for a continuous wave. Figure 7 plots the attenuation as a function of the Seki parameter and shows that for $S < 0.1$ the estimated attenuation due to diffraction will be less than 0.59 dB, which represents a loss of 13%. For the cases considered in this report the Seki parameter is less than 0.1 indicating small diffraction losses.

The radial symmetry of a piezoelectric disk allowed Johansson *et al* [27] to investigate 3-dimensional diffraction effects with a 1-dimensional model, however it is more difficult to incorporate other, non-symmetric, 3-dimensional effects into a 1-dimensional LTSpice model. In particular, it is believed that small non-uniform variations in layer thicknesses (e.g. bondline, piezoelectric material, metal plate) have a significant effect on the behaviour of an AEF system and would be a challenge to simulate with a 1-dimensional model. Due to time constraints average thickness values have been used in the current modelling.

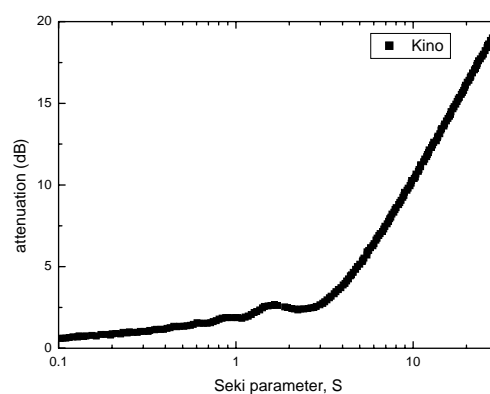


Figure 7: Attenuation caused by diffraction, after Johansson [27] and Kino [28]

The LTSpice modelling is optimised for the first thickness mode as described by Püttmer *et al* [14]. Practically this meant that a constant frequency-independent resistance value was chosen for each of the lossy transmission lines that are used to model damping in the piezoelectric

elements, the metal plate, and the bondlines. Lossy transmission line resistance, R_{TL} , is calculated using [15],

$$R_{TL} = \frac{\omega_{AR} L}{Q} \quad (3)$$

where $L = \rho A$, $A = \pi R^2$, $\omega_{AR} = 2\pi f_{AR}$ and the anti-resonant frequency $f_{AR} = v_D/(2H)$ as given by [20].

The assumption of a constant R_{TL} implied by equation 3 meant the mechanical Q values used in the LTSpice modelling were only correct at the anti-resonant frequency f_{AR} , and the mechanical Q values for all materials effectively increased as the frequency was increased. In other words, the assumption of a constant R_{TL} over-estimates the material damping below f_{AR} and under-estimates the material damping above f_{AR} .

The silver-epoxy material properties determined by Rajic [24] were calculated at ~ 4 MHz. The LTSpice modelling in this paper assumed that the mechanical damping of silver epoxy was frequency independent. The authors are aware however that the damping properties of visco-elastic materials can vary quite markedly with frequency. For example, van Deventer *et al* [15] shows that the mechanical Q of PMMA increases from 10 to 100 over the 10 Hz - 10 MHz frequency range.

2. Experimental

This section examines the manufacture of the various AEF arrangements and the subsequent experimental investigations. Figure 8 shows two schematics of the experimental configurations utilised to examine the behaviour of the AEF arrangements. Two *well matched* Pz27 disks with 38 mm diameter and 2 mm thickness were chosen (where *well matched* meant that the two Pz27 disks had well matched fundamental thickness-mode resonance and anti-resonance peaks). Silver-cement was used as the electrode material for the Pz27 disks because it is easily soldered. The disks were bonded to either side of the metal plates using silver loaded epoxy [23] with the disk centres axially collocated to within ± 1 mm. The steel plate used had dimensions of 100 mm by 64 mm by 6 mm thick, whereas the aluminium plates were square with a side length of 600 mm.

The AEF systems were prepared using the following procedure:

(i) *Impedance measurements.* A Solartron SI-1260 impedance analyser was used with a custom-built PZT measuring attachment (shown in Figure 9a and b). Impedance spectra were measured to ensure that the two Pz27 disks (Transmit and Receive) were well matched in terms of their through-thickness resonance and anti-resonance. During the impedance measurements the samples were mounted with the loaded *gold pogostick* contacting the centre of the disk (see Figure 9).

Impedance data was collected over the frequency range 1 kHz to 10 MHz, sampling at 1000 points per decade, with 1 second temporal averaging per point. The impedance frequency

sweep was collected near the thickness resonance at maximum frequency resolution to accurately determine the frequency location of the thickness resonance and anti-resonance. If the thickness resonances (and anti-resonances) of the two disks were not well matched (i.e. differed by more than ± 500 Hz) then the process was repeated until two matching samples were found. Matching of the two disks will be discussed in more detail later in this report.

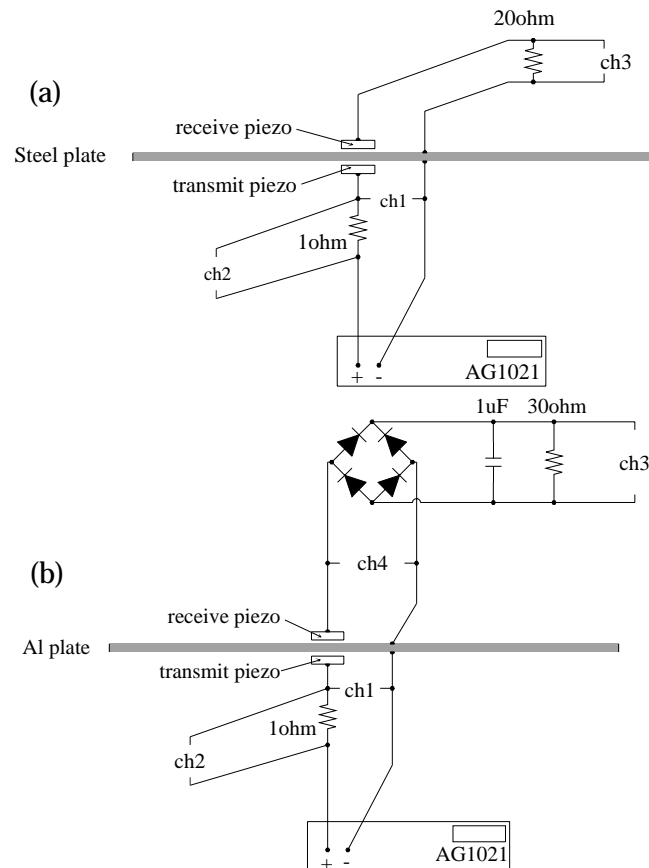


Figure 8: Schematic of the AEF power transfer experimental arrangements for (a) steel plate (b) aluminium plate

(ii) *Soldering electrical contacts to the PZT disks.* A fine-point soldering iron was set to just over $360\text{ }^{\circ}\text{C}$. Flux was applied to a small area at the centre of a Pz27 disk. A 10 mm length of solder was melted onto the clean soldering iron tip and the tip was then quickly ‘dabbed’ onto the Pz27 surface. It was found that excessive heat or delay whilst applying the solder would cause the silver metallization (on the Pz27 surface) to be subsumed into the solder ball.

(iii) *Plate surface preparation.* The area of plate to be bonded was gently cleaned with acetone and followed by ethanol to remove any acetone residue. The bonding area was then scored in the vertical direction using 600 grade wet-and-dry abrasive paper with ethanol lubricant (allowing extra area for the silver-epoxy spew fillet). The number of scoring strokes was kept to a minimum to reduce material loss from the surface of the plate. Scoring was repeated in the horizontal direction, again keeping the number of strokes to a minimum. Ethanol was

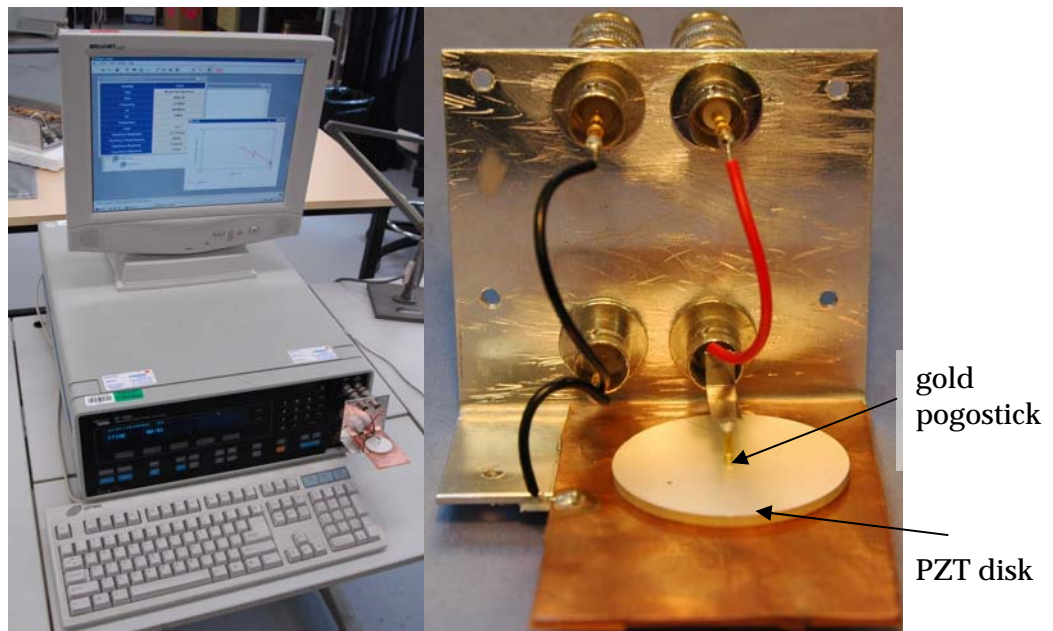
used to remove residue from the abrasive paper. The bonding area was cleaned with acetone and again the acetone residue was removed with ethanol.

(iv) *Bonding of the Pz27 disk.* The CW2400 silver loaded epoxy [23] was prepared according to the manufacturers instructions. The instructions stated that the pot-life after mixing is 10 minutes, however the authors found that the useful working time of the epoxy was approximately 5 minutes. Additionally, the instructions state that mixing should take 2 minutes, however for small quantities the authors found 1 minute to be sufficient, which allowed extra working time for placement of the Pz27 disk onto the bonding area. A spatula was used to apply a uniform layer of the mixed epoxy to the underside of the Pz27 disk which was then immediately placed on the plate. Using gloved fingers, pressure was applied to the disk and a small circular motion was used to ensure that the epoxy spew fillet was uniformly distributed around the circumference of the disk. A scalpel was used to remove excess epoxy from the edge of the disk, however the spew-fillet was left intact during this process. It was found that removing the excess at this stage simplified the process of eliminating electrical shorts after curing. Figure 10 shows an example of a 38 mm diameter, 2 mm thick Pz27 disk bonded to an aluminium plate.

(v) *Curing of the silver epoxy.* After the Pz27 disk was satisfactorily positioned it was covered with Teflon sheet and approximately 500 grams of mass was applied. According to the manufacturer the epoxy should be cured at room temperature (24 °C) for 4 hours, or at a temperature of 66 °C (to 121 °C) for 10 minutes. To ensure maximum bond strength the authors used a 250 W heat lamp, which produced a sample temperature of 60 °C, for 2 hours and then allowed the sample to sit at room temperature for at least 24 hours.

(vi) *Removal of electrical shorts.* After curing a multi-meter was used to test for electrical shorting between the top Pz27 electrode and the plate. If a short had occurred a Q-tip and a very small amount of acetone was used to remove excess epoxy from the edge of the Pz27 disk, with care taken to ensure that the acetone did not contact or flow down to the spew fillet and hence weaken the bond.

Steps (ii) to (vi) were repeated to bond the second Pz27 disk to the opposite side of the plate. With the two Pz27 disks (transmit and receive) bonded to the plate and cured, the simple circuits shown schematically in Figure 4 (or Figure 5) were built. An AG1021 100 W power amplifier was used to drive the transmitting Pz27 disk. A 4-channel oscilloscope with floating probes was connected to monitor the input voltage and current used to drive the transmit Pz27 disk, the voltage across the load resistor and, if a diode bridge was used on the receive side, the output voltage across the receive Pz27 disk was also measured. Drive frequency was stepped across the range of interest (normally 400 kHz to 1300 kHz), with the amplifier output adjusted at each step to give the required apparent input power to the transmit Pz27 disk.



(a) (b)
Figure 9: Impedance measurements using (a) Solartron 1260 and (b) the DSTO piezoelectric disk adaptor

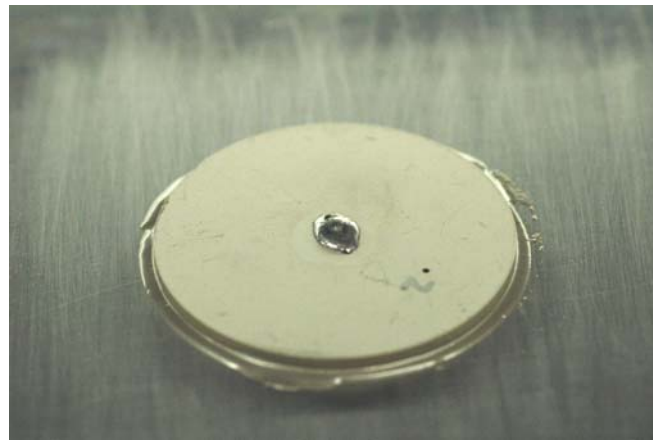


Figure 10: Pz27 element immediately after silver-epoxy bonding to aluminium plate

3. Results and Discussion

In the following, Part 1 develops the LTSpice AEF model, extends the model to include bondlines and then compares the predictions with those found in the literature while Part 2 utilises the LTSpice AEF model to investigate geometrical and material parameters with the aim of optimizing power transfer through an aluminium skin. Part 2 also includes a comparison with experimental data.

3.1 Part 1 - Steel plate Acoustic Electric Feedthrough

The AEF geometry under investigation is that considered by [9, 10] and involves 6 mm thick steel plate with PZT disks of 1 mm and 2 mm thickness bonded to either side of the plate. The LTSpice model in Figure 4 was developed to reproduce this and to also examine the effect of silver-epoxy bondlines. Material parameters for modelling were extracted from the literature and are given in Appendix C. The LTSpice model was optimised for the thickness anti-resonant mode of the 1 mm thick transmit piezoelectric disk located at a frequency of approximately 2 MHz. Figure 4a shows the locations of V_{out} and V_{in} and Figure 11a compares V_{out}/V_{in} curves reproduced from the literature [9] with those produced using the model given in Figure 4.

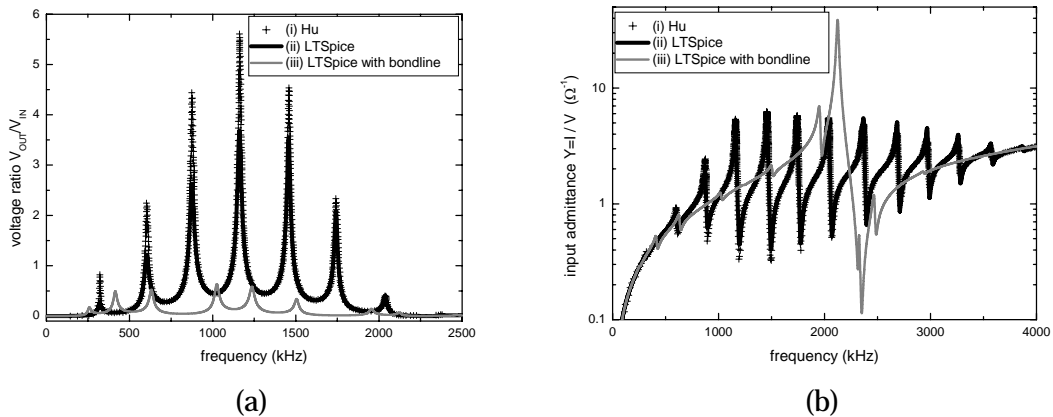


Figure 11: Simulation results comparing (a) the voltage ratios and (b) the admittance for three cases: (i) literature reproduced from Hu et al [9], (ii) LTSpice modelling using lossy transmission line damping models for the piezoelectric and steel elements and (iii) the LTSpice model with 100 μm silver epoxy bondlines added between the piezoelectric elements and the steel

The lossy transmission lines utilised in the LTSpice AEF modelling were more sophisticated than the damping models utilised in the literature [9, 10]. The use of more sophisticated damping models resulted in smaller resonant peaks, as shown in Figure 11a. Figure 11a also shows the effect of adding two 100 μm bondlines (i.e. one bondline on each side of the steel plate) to the LTSpice model, resulting in further substantial suppression of the resonant peaks (with peak voltage ratios $V_{OUT}/V_{IN} < 1$) which were also shifted in frequency. Figure 11b shows a comparison of the input admittance curve from the literature and those modelled

using LTSpice and again the addition of the two 100 μm bondlines has a significant effect on the behaviour of the AEF model.

The initial AEF modelling was carried out using piezoelectric material parameters extracted from the literature [9, 10]. To extend the modelling and hence allow comparison with measured AEF data it was necessary to show that the LTSpice piezoelectric model could accurately predict the thickness mode resonance behaviour of the Pz27 disks used. The piezoelectric LTSpice model shown in Figure 1b was hence created to confirm that the three port piezoelectric model found in the literature was suitable. Note that the LTSpice model was optimised for the first thickness mode, as discussed in [14].

Impedance spectra from the model were compared with measured impedance spectra that were collected using a custom built sample holder, shown in Figure 9. Figure 12 shows the measured impedance data from a free Pz27 disk, 38 mm diameter and 2mm thick, over the range 1 kHz to 10 MHz; plotted near 1 MHz is the modelled impedance data computed using the LTSpice model of a Pz27 disk shown in Figure 1b.

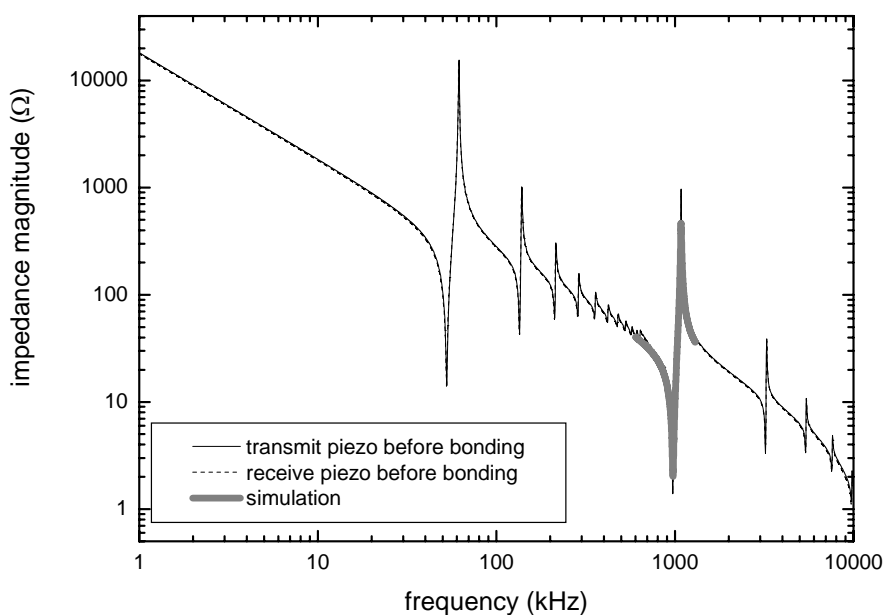


Figure 12: Measured impedance magnitude spectrum over the frequency range 1 kHz-10 MHz, and modelled data in the vicinity of the fundamental through-thickness resonance (~972 kHz)

The series of measured resonance peaks located between ~50 kHz and 600 kHz are lateral vibrations (in the 1 direction) that are not modelled in the LTSpice Pz27 simulation, which only models thickness-mode resonances. Figure 13 examines the frequency range near the thickness-mode resonance and shows that excellent agreement was found between the measured and modelled magnitude and phase. Figure 13 also shows that mode coupling occurs between the radial and thickness modes. Noting that impedance is the reciprocal of

admittance, to facilitate comparison of Figure 2 with Figure 13a, the thickness mode resonance has been marked with T and the radial coupled modes are labelled R. As discussed earlier, the observed mode coupling was confirmed by the manufacturer [21].

Having confirmed the LTSpice piezoelectric model was predictive the model was then applied to the AEF geometry considered in [9] and [10], after which an experimental validation was performed. Two Pz27 disks, 38 mm diameter, with thicknesses of 1 mm (transmit) and 2 mm (receive) were bonded to either side of a small steel plate, with dimensions 100 mm x 64 mm x 6 mm thick. A 20 Ω linear load resistance was attached to the receive Pz27 disk as shown schematically in Figure 4. The apparent input power for the experiment was limited to 500 mW as higher input powers were found to distort the output load voltage.

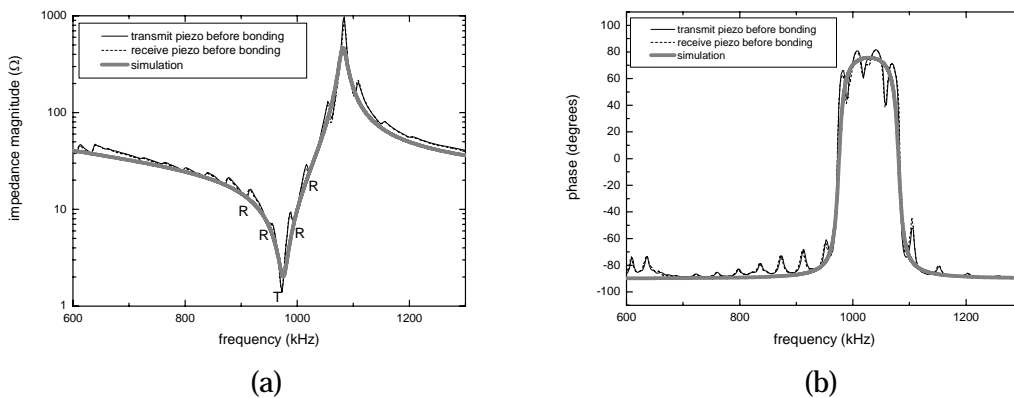


Figure 13: Comparison of measured and modelled (a) impedance magnitude and (b) phase near the thickness resonance, where thickness mode resonance has been labelled with T and the radial coupled modes are labelled R

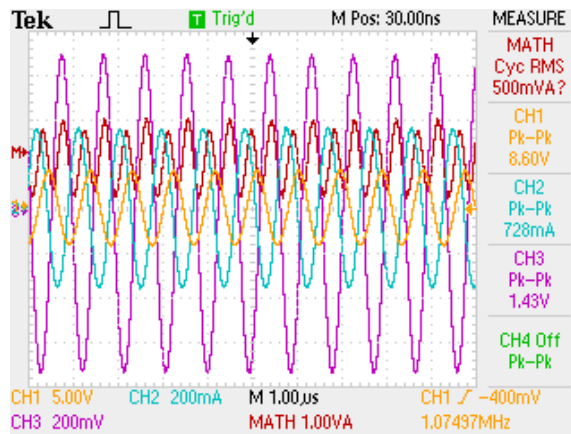


Figure 14: Oscilloscope screen capture showing three traces from steel plate AEF experiment. Channel locations are indicated in Figure 8a: Ch1=V(in), Ch2=I(R2), Ch3=V(out) across 20 Ω

Figure 14 shows an example oscilloscope trace measured at a drive frequency of 1075 kHz near the anti-resonance frequency of the 2 mm thick Pz27 disk in the steel plate AEF. An oscilloscope trace was captured at each drive frequency step shown in Figure 15. Using the oscilloscope traces it was possible to find the power transfer efficiency ν , defined as,

$$\nu = 100 \times \left(\frac{P_{RECEIVE}}{P_{TRANSMIT}} \right) \quad (4)$$

where $P_{TRANSMIT} = V(in) \times I(R2)$ and $P_{RECEIVE} = V(out) \times I(R1)$

Figure 15 shows a comparison of measured power transfer efficiencies with those found using LTSpice simulation. For the purpose of modelling, nominal 100 μm silver-epoxy bondlines were chosen. The experimental efficiency was calculated using $P_{TRANSMIT} = 500 \text{ mW}$ and $P_{RECEIVE} = (V_{RMS}^{LOAD})^2 / 20\Omega$. Figure 15 shows that both the measured and modelled peak power transfer efficiencies were quite poor, less than 2%, for this geometry and load resistance.

Subsequent micrometer measurements revealed that the thickness of the steel plate varied from 5.80 mm at the edge of the plate to 5.99 mm at the middle. Given that there was a 200 μm thickness variation across the plate it was not expected that the frequencies of the measured resonance peaks would match those computed by the one-dimensional LTSpice simulation, which assumed uniform bondlines and plate thicknesses. The authors expected that the thickness variation of the steel plate would mean that a full three-dimensional model would be required to satisfactorily model the AEF system, however Figure 15 does seem to show reasonable correlation between the measured and modelled resonant peaks at 625 kHz and 1025 kHz.

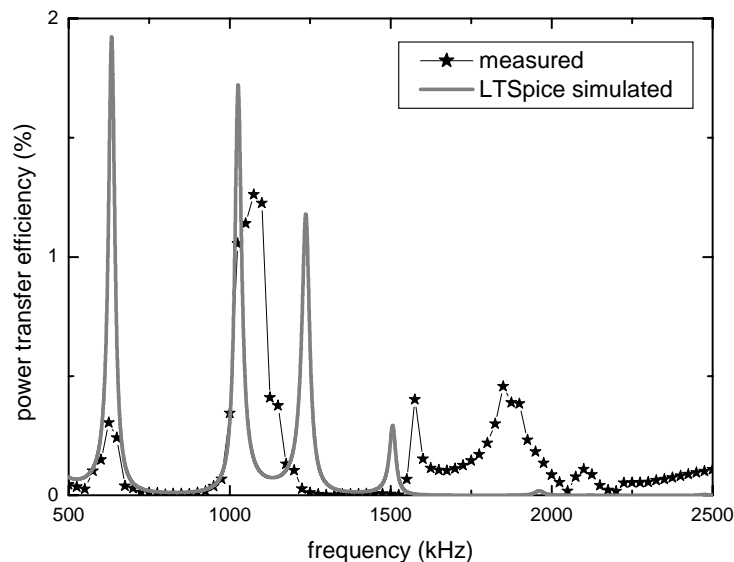


Figure 15: Measured versus modelled power transfer efficiency for a 1 mm Pz27/6 mm steel/2 mm Pz27 AEF system. Note the peaky nature of the plot with very low power transfer between the peaks.

The AEF efficiency curves given in the literature [9, 10] show significant power transfer in between the resonant peaks, however with more realistic damping in the AEF model the efficiency curves became peaky with very little power transfer between the resonant peaks. It is also worth noting that the efficiencies shown in Figure 15 are substantially lower than the predictions found in the literature so it is clear that using lossy transmission lines to model damping and adding the adhesive bondlines has a significant effect on the power transfer efficiency.

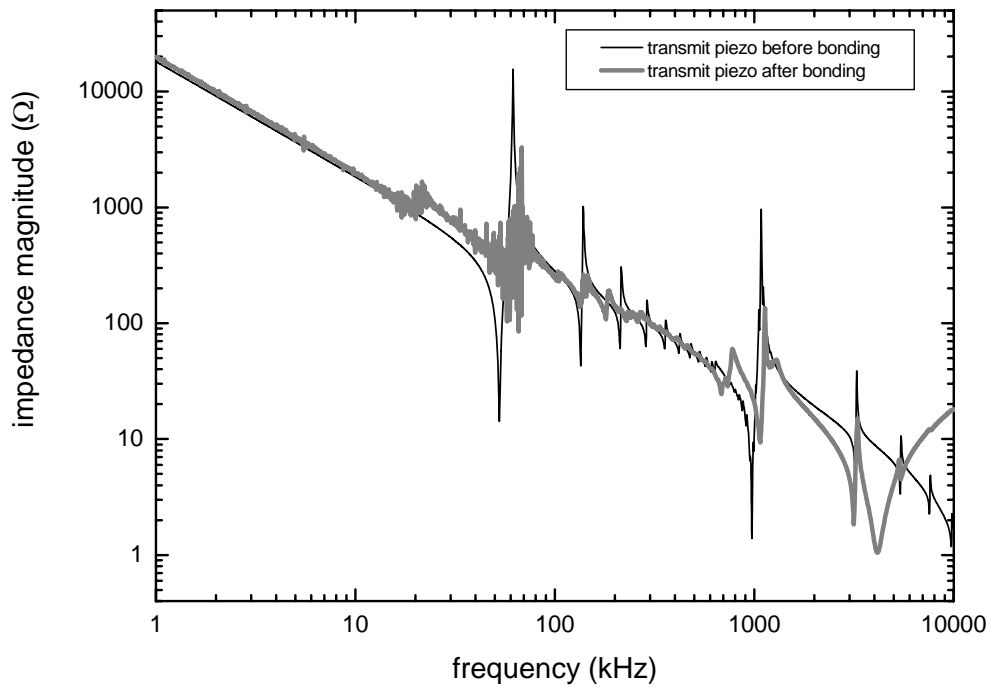
3.2 Part 2 - Aluminium plate Acoustic Electric Feedthrough

The ultimate goal of this research is the development of an AEF system to provide power and communications through the skin of an aircraft. With the LTSpice AEF model agreeing satisfactorily with the literature and also shown to have predictive capability, an investigation of AEF power transfer through aluminium plate was undertaken.

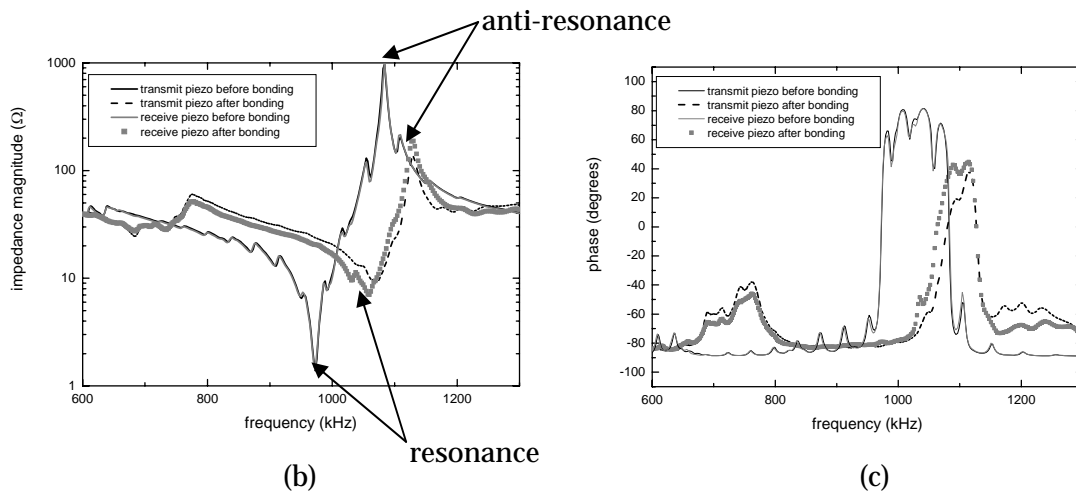
Prior to modelling the aluminium plate AEF system a series of impedance curves were measured before and after bonding Pz27 disks (38 mm diameter and 2 mm thick) to a 1.6 mm thick aluminium plate. The results of these measurements are shown in Figure 16. Figure 16a shows impedance curves taken over the frequency range 1 kHz to 10 MHz and compares the impedance of the transmit Pz27 disk before and after bonding to a 1.6 mm thick aluminium plate. As might be expected, bonding the Pz27 disks to a metal plate resulted in the attenuation and shifting of the radial resonance peaks located between 50 kHz and 600 kHz. The thickness resonance modes seen at 1 MHz and above were also attenuated and shifted (to a higher frequency) after bonding. Figure 16b shows that the fundamental thickness resonance of both the transmit and receive Pz27 disks shifted to a higher frequency after bonding, i.e. from 972 kHz to ~1060 kHz.

Close examination of Figure 16b reveals that the anti-resonant frequencies of both the transmit and receive Pz27 disks was 1084 kHz prior to bonding and shifted to 1129 kHz after bonding. Figure 16c shows that, prior to bonding, the transmit and receive Pz27 disks had extremely well matched resonance and anti-resonance frequencies with the centre of the phase peak located at ~1027 kHz and that, after bonding, the peak shifted to ~1100 kHz. Prior to bonding the mode coupling between the thickness and radial modes is clearly visible in Figure 16b and Figure 16c which also show that the mode coupling was severely attenuated after bonding.

Simulations were carried out using the LTSpice AEF model in Figure 5 and comparison was made with laboratory data measured using the experimental setup (Figure 8b). An example of a measured oscilloscope trace is shown in Figure 17; similar traces were captured at each step in drive frequency. The measured data presented in Figure 18, 19 and 20 was calculated from traces similar to Figure 17.



(a)



(b)

(c)

Figure 16: Impedance measurements of 2 mm thick Pz27 disks before and after bonding to 1.6 mm Al plate: (a) shows the measured impedance magnitude from the transmit piezoelectric element, for both transmit and receive piezoelectric elements (b) shows details of the measured impedance magnitude near the fundamental thickness resonance and (c) the corresponding phase

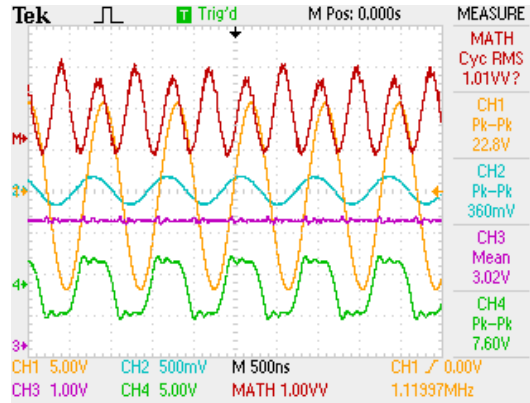


Figure 17: Oscilloscope screen capture showing four example voltage traces from the aluminium plate AEF experiment. Channel locations are indicated in Figure 8b: Ch1= $V(in)$, Ch2= $I(R2)$, Ch3= $V(out)$ across $30\ \Omega$, Ch4= $voltage$ across the receive piezo

Figure 18a is the modelled and measured load voltage as a function of frequency for an AEF formed using 1.6 mm thick aluminium plate, showing a modelled peak voltage of ~ 4 V and a measured peak voltage of ~ 3 V. Plotted in Figure 18b are curves of load power as a function of frequency. Since the load voltage had a negligible amount of ripple the power was estimated using the simple relationship $P_{LOAD} = (V_{MEAN}^{LOAD})^2 / 30\Omega$. The modelled peak power transfer was near 550 mW whilst the measured peak power transfer was just over 300 mW. It is assumed that the difference is the power lost to the metal plate which is not included in the model. The approximate power transfer efficiency $\nu = 100 \times (P_{LOAD} / 1)$, shown as a percentage in Figure 18b, is only accurate at the resonant peaks where the real input power was about 1 W.

Figure 18b also shows that the maximum measured power transfer peak was centred near 1100 kHz with a Full-Width-Half-Maximum (FWHM) of ~ 166 kHz while the maximum modelled power transfer peak was centred at 1091 kHz with FWHM ~ 183 kHz. Both the modelled and measured power curves show that the centre of the maximum power transfer peak was located near the anti-resonant frequency of a bonded 2 mm thick Pz27 disk (Figure 16) which is expected since losses within the disk are minimised at anti-resonance. The phase plot between input current and drive voltage shown in Figure 19 gives an indication as to why the resonance peak near 1100 kHz was so wide. The modelled phase data shows three clearly discernable peaks located side by side near 1100 kHz which indicates that there may be a similar number of peaks present between 1000 kHz and 1200 kHz in the measured phase data.

Modelled and measured results pertaining to a 5 mm thick aluminium plate are shown in Figure 20 and are quite similar to those in Figure 18 for the 1.6 mm thick plate. In particular, the peak values of the modelled and measured load voltage (and power) at ~ 1040 kHz are close to those found for the 1.6 mm plate near 1100 kHz.

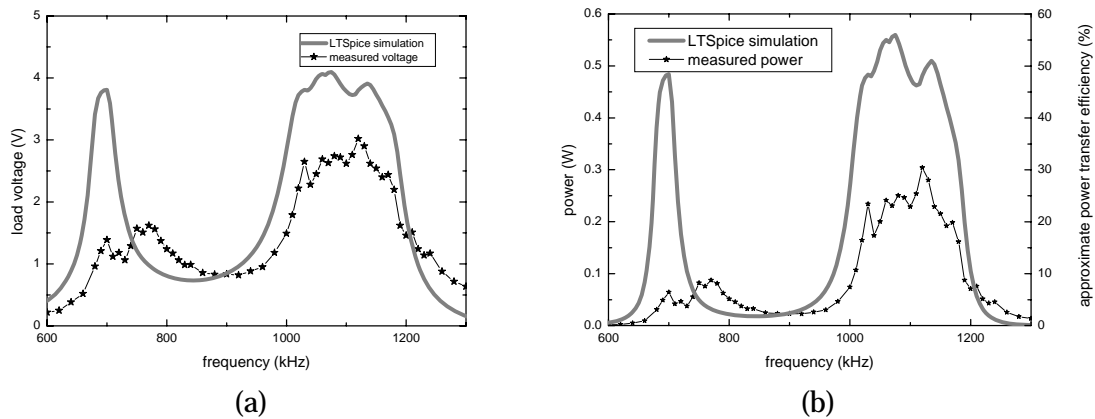


Figure 18: Measured and modelled results for the 2 mm Pz27/1.6 mm Al/2 mm Pz27 AEF configuration (a) load voltage and (b) transmitted power as a function of frequency

To examine the effect of metal plate thickness on the power transfer efficiency a series of simulations, varying the input drive frequency and the aluminium plate thickness, were run using the LTSpice model shown in Figure 5. Again, 38 mm diameter, 2 mm thick Pz27 disks were used to form the AEF system. Figure 21 shows the load voltage response for a range of fixed drive frequencies for varying aluminium plate thickness. From Figure 21 it can be inferred that for drive frequencies near the 1100 kHz anti-resonance, the thickness of the aluminium plate has little effect on the amount of power transferred through the plate. This prediction is borne out in practice as shown in Figure 18 and Figure 20 where the measured power transfer efficiency was found to be similar for aluminium plate thicknesses of 1.6 mm and 5 mm. Of course as plate thickness increases diffraction effects (i.e. Figure 7) become important and would reduce the power transfer efficiency.

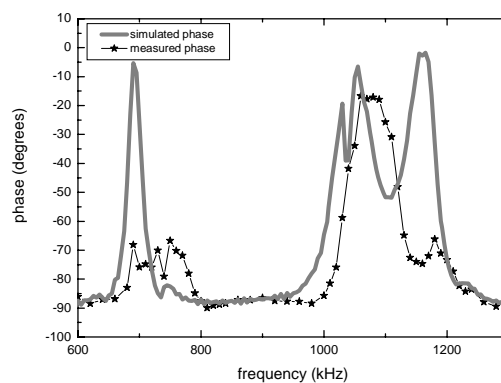


Figure 19: Phase spectra for a 2 mm Pz27/1.6 mm Al/2 mm Pz27 AEF configuration

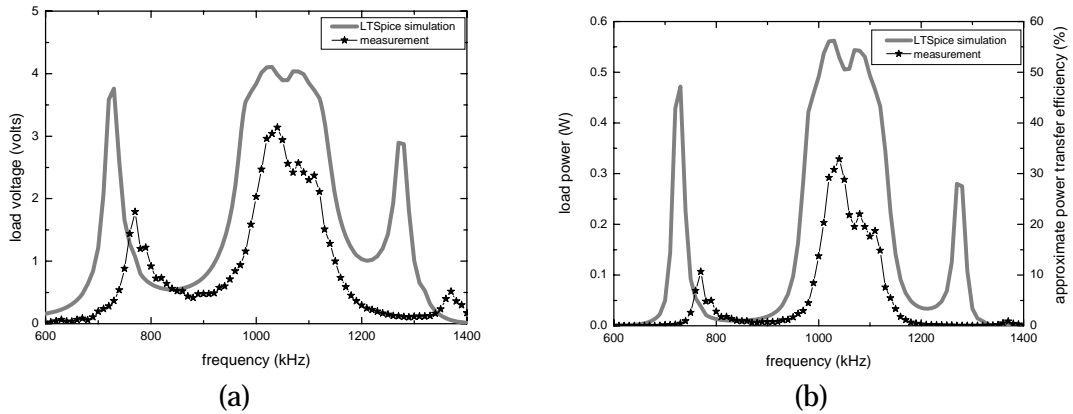


Figure 20: Measured and modelled results for the 2 mm Pz27/5 mm Al/2 mm Pz27 AEF configuration, (a) load voltage and (b) transmitted power as a function of frequency

For drive frequencies away from 1100 kHz (i.e. for frequencies away from the anti-resonance) there appeared to be a particular set of thicknesses that allowed maximum power transfer. For example, Figure 21 indicates that a drive frequency of 900 kHz produces maximum power transfer through plates of 0.6 mm and 3.5 mm thickness.

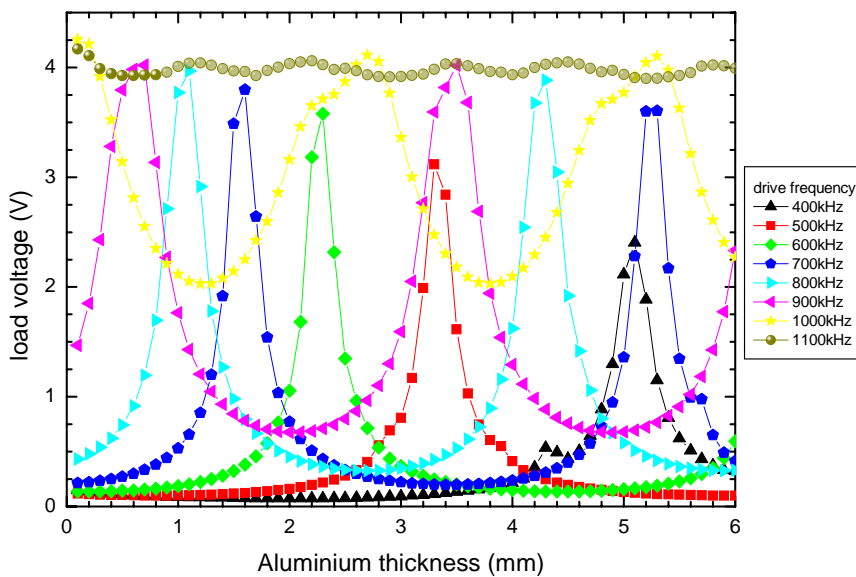


Figure 21: Modelled results for an AEF system with varying plate thickness and drive frequency using a 1 W constant apparent input power and a 30 Ω load resistor

The LTSpice model in Figure 5 was modified to investigate the effect of the piezoelectric element thickness on the power transferred through a 1.6 mm aluminium plate. The load resistor R1 was removed and the voltage across the 1 μF storage capacitor C1 was measured

as a function of time. Both the transmit and receive piezoelectric elements used in the AEF system had the same nominal thickness. The input drive frequency was adjusted to be equal to the resonance frequency for each element thickness modelled. Figure 22a shows the modelled steady state load voltage as a function of Pz27 disk thickness. The actual voltages plotted in Figure 22a are 90% of the final steady state $C1$ capacitor voltage, $V_{90\%}$; this value was chosen to keep simulation times reasonable.

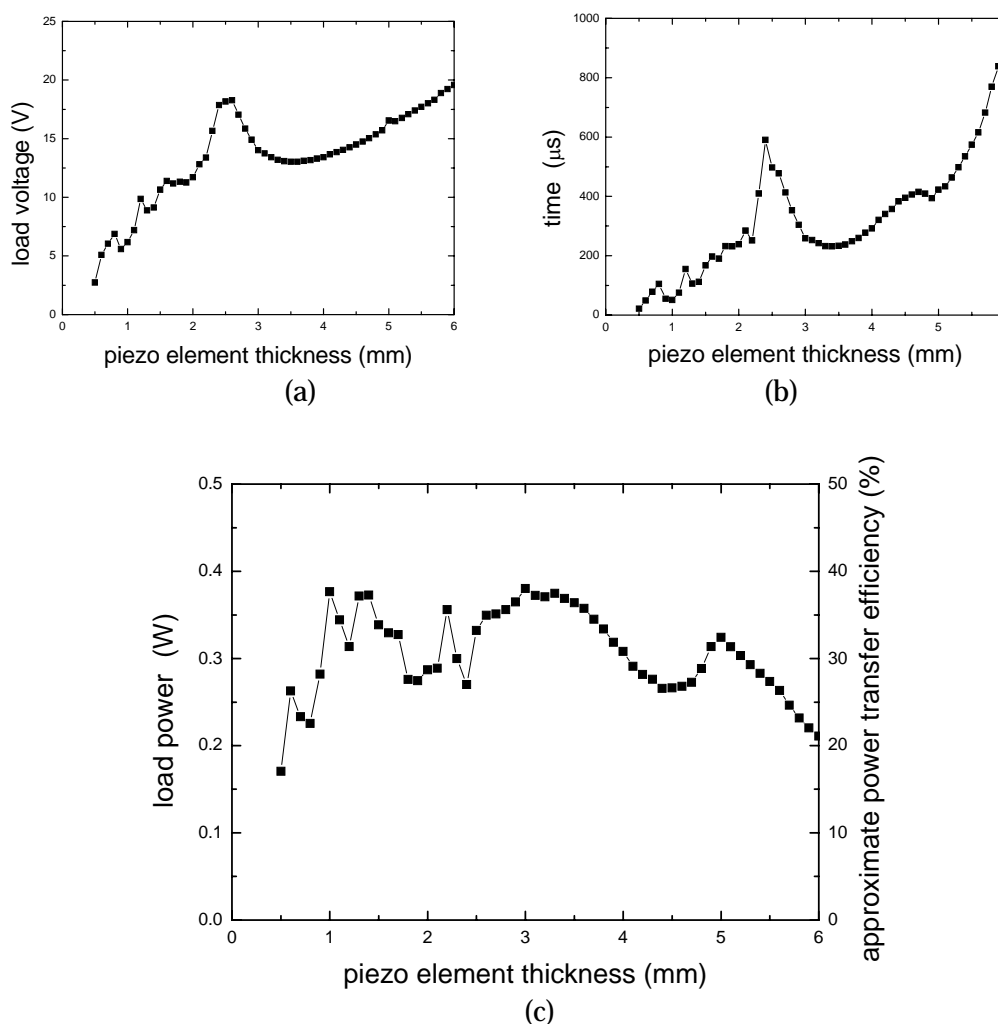


Figure 22: Modelled results for an AEF system for a 1.6 mm thick Al plate, where the PZT element thickness is varied: (a) 90% of steady state load voltage, (b) time taken to reach 90% of steady state load voltage, and (c) load power as a function of varying Pz27 thickness

The time taken for the $C1$ capacitor to reach 90% of its steady state voltage, $t_{90\%}$, is plotted in Figure 22b. Figure 22c plots load power as a function of piezo element thickness, where load power was calculated using,

$$P_{LOAD} = \frac{1}{2} \frac{C(V_{90\%})^2}{t_{90\%}} \tag{5}$$

where $C=C1=1 \mu\text{F}$.

The load power plotted in Figure 22c is not power in the true sense, but is the power stored and consumed in the following cycle:

- (i) a *capacitor charge cycle* (where the load is capacitive only) is followed by,
- (ii) an *energy use cycle* during which the energy stored in the capacitor in stage (i) is dissipated through a real load.

Figure 22c shows a trend towards lower power-transfer efficiency for piezoelectric element thicknesses below 1 mm. For a 1.6 mm aluminium plate Figure 22c suggests that a range of piezoelectric element thicknesses from 1 mm to 3 mm could be used to form an AEF system with power transfer efficiencies in the range of 25-40%.

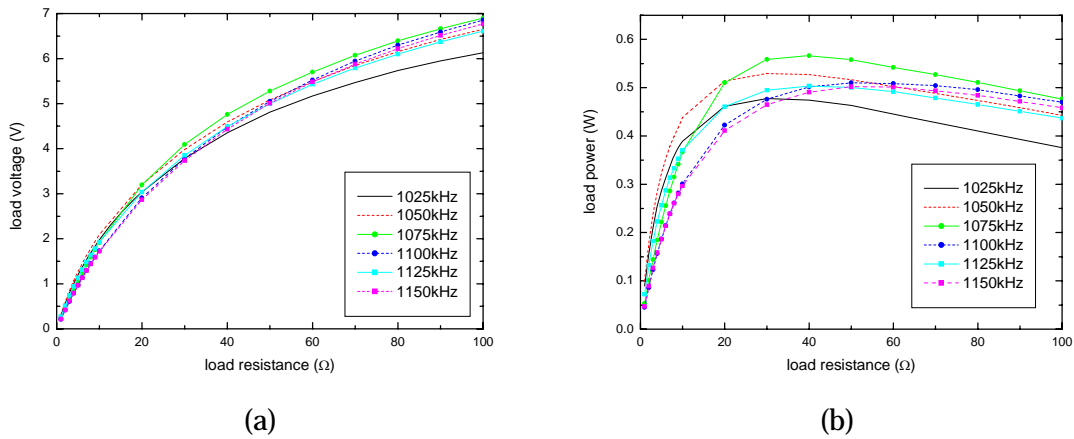


Figure 23: Modelled results for 2 mm Pz27/1.6 mm Al/2 mm Pz27 AEF configuration, (a) load voltage and (b) load power, with varying load resistance and drive frequency swept across the fundamental thickness resonance, 1025-1150 kHz

Finally, the reason for choosing a 30 Ω load resistance for the aluminium plate AEF configuration is apparent in Figure 23 which plots a series of simulation results where both the load resistance and drive frequency were varied. The LTSpice model shown in Figure 5 was again modified and this time resistor R1 was stepped across the range 1 Ω to 100 Ω and the input drive frequencies were stepped from 1025 kHz to 1150 kHz, corresponding to the main power-transfer peak as shown in Figure 18 and Figure 20. Figure 23 shows that a 30 Ω load resistor produced load voltages from 3.7 V to 4.1 V which was deemed to be a useful voltage range by the authors. However, more importantly it appears that the load resistance for optimum power transfer efficiency lies somewhere in the range of 30 Ω to 60 Ω and is somewhat independent of the drive frequency as long as it is within approximately ±50 kHz of the thickness-mode resonance.

4. Conclusion

The Acoustic Electric Feedthrough (AEF) technique was investigated as a possible means of passing power through the aluminium skin of an aircraft. An AEF operates using two axially aligned piezoelectric elements, located on opposite sides of a metal plate. A piezoelectric element excited at its thickness mode anti-resonant frequency is used to transmit ultrasound through a metallic plate. The ultrasound is received by a second element located on the opposite side of the plate. An LTSpice model of the AEF scheme was developed and used to reproduce and extend modelling found in the literature. In particular, the model included lossy transmission lines to represent material damping in the AEF scheme and silver epoxy bondlines. The effect of these additions was to significantly dampen ultrasonic standing waves created in the AEF system which resulted in reduced power transfer efficiencies compared with theoretical results reported in the literature. The LTSpice model was used to investigate an AEF system installed on aluminium plate and the simulation results were compared with the results from the experiment. Modelling and experimentation was carried out with two piezoelectric elements (transmit and receive) that were well matched, meaning that they had near identical resonance and anti-resonant thickness modes. It was shown that if the drive frequency was equal to the anti-resonant frequency of the piezoelectric elements used to create the AEF system, then the power transfer efficiency was unaffected by plate thickness. Using Pz27 disks, of 38 mm diameter and 2 mm thick, laboratory testing has shown that with 1 W of input power then 300 mW of real power could be transmitted to an electrical load through aluminium plates of 1.6 mm and 5 mm thickness. Future work will involve both the investigation of various types of piezoelectric materials to determine the optimum ceramic composition for power transfer and the development of AEF-based communications techniques.

5. References

1. S. C. Galea, S. van der Velden, S. Moss, I. Powlesland, "On the way to autonomy: the wireless-interrogated and self-powered 'smart patch' system," (to be published in *Encyclopaedia of Structural Health Monitoring* by Wiley)
2. S. D. Moss, S. C. Galea, I. G. Powlesland, M. Konak, A. A. Baker, "In-situ health monitoring of a bonded composite patch using the strain ratio technique," *SPIE's 2000 Symposium on Smart Materials and MEMS, Smart Structures and Devices Conference*, Melbourne, Australia, SPIE 4325, 2000; Paper 4235-41.
3. S. C. Galea, S. D. Moss, I. G. Powlesland, A. A. Baker, "Application of a Smart Patch on an F/A-18 Aileron Hinge," *Proc ACUN - 4 Composite Systems - Macrocomposites, Microcomposites, Nanocomposites*, UNSW, SYDNEY, Australia, 2002.
4. C. Davis, W. Baker, S. Moss, S. Galea, R. Jones, "In situ health monitoring of bonded composite repairs using a novel fiber Bragg grating sensing arrangement," *Proceedings of SPIE -- Volume 4934, Smart Materials II*, Alan R. Wilson, Editor, November 2002, pp. 140-149
5. N. Rajic, "In situ Monitoring of Crack Growth in Mild Steel under Closure Conditions Using a Piezotransducer Array," *Journal of Intelligent Material Systems and Structures*, Vol. 11, No. 9, 696-702 (2000)
6. R. Bartholomeusz, B. Crawford, C. Davis, S. Galea, B. Hinton, G. McAdam, I. Powlesland, K. Sharp, P. Trathen, T. Trueman and A. Wilson, "DSTO Aircraft Structural Prognostic Health Monitoring Program for Corrosion Prevention and Control," *Corrosion & Prevention - 2004 Australasian Corrosion Association Inc.*, Perth, November 21-24 2004, Perth, WA
7. C. P. Gardiner, P. Vincent, A. Wilson, D. Ellery, and T. Armstrong, "A trial sensor network for the Armidale Class Patrol Boat," *Pacific 2008 International Maritime Conference*, Sydney, Australia, January 2008
8. P. S. Vincent, P. J. McMahon, R. F. Muscat, L. Zeve, A. R. Wilson, "A small low-power networked and versatile sensor interface (*Invited Paper*)," *SPIE International Symposium on Smart Materials, Nano-, and Micro-Smart Systems 2006: Smart Structures, Devices and Systems III*, December 2006, [6414-39]

-
9. Y. Hu, X. Zhang, J. Yang, Q. Jiang, "Transmitting Electric Energy Through a Metal Wall by Acoustic Waves Using Piezoelectric Transducers," *IEEE Trans. Ultrason., Ferroelect., Freq. Cont.*, vol. 50, no. 7, pp. 773-781, 2003
 10. S. Sherrit, M. Badescu, X. Bao, Y. Bar-Cohen, Z. Chang, "Efficient electromechanical Network Models for Wireless Acoustic-Electric Feedthroughs," *Proceedings of SPIE Smart Structures Conference, San Diego, CA., Mar 6-10, 2005*, SPIE vol. 5758
 11. M. Engelhardt, LTspice/SwitcherCAD III, Linear Technology Corporation, www.linear.com, 2008
 12. S. A. Morris, C. G. Hutchens, "Implementation of Mason's Model on Circuit Analysis Programs," *IEEE Trans. Ultrason., Ferroelect., Freq. Cont.*, vol. UFFC-33, no. 3, pp. 295-298, 1986
 13. W. M. Leach Jr., "Controlled-Source Analogous circuits and SPICE Models for Piezoelectric Transducers," *IEEE Trans. Ultrason., Ferroelect., Freq. Cont.*, vol. 41, no. 1, pp. 60-66, 1994
 14. A. Püttmer, P. Hauptmann, R. Lucklum, O. Krause, B. Henning, "SPICE Model for Lossy Piezoceramic Transducers," *IEEE Trans. Ultrason., Ferroelect., Freq. Cont.*, vol. 44, no. 1, pp. 60-66, 1997
 15. J. van Deventer, T Löfqvist, "PSPICE Simulation of Ultrasonic Systems," *IEEE Trans. Ultrason., Ferroelect., Freq. Cont.*, vol. 47, no. 4, pp. 1014-1024, 2000
 16. L. Wu, Y-C. Chen, "PSPICE approach for designing the ultrasonic piezoelectric transducer for medical diagnostic applications," *Sensors and Actuators A*, vol. 75, pp. 186-198, 1999
 17. W. P. Mason *Electromechanical Transducers and Wave Filters*, 1st edn (Princeton, NJ: Van Nostrand) 1948
 18. R. Krimholtz, D. A. Leedom and G. L. Matthaei, "New equivalent circuit for elementary piezoelectric transducers," *Electron Lett.*, vol. 6, pp. 398-9, 1970
 19. M. Kim, J. Kim, W. Cao, "Aspect ratio dependence of electromechanical coupling coefficient of piezoelectric resonators," *App. Phys. Lett.*, vol. 87, pp 132901-1 to 132901-3, 2005

-
20. D. A. Berlincourt, D. R. Curran and H. Jaffee, *Physical Acoustics Principles and Methods, Volume I - Part A*, pp.170-267 (Academic Press, New York and London, 1964), Library of Congress Catalog Card Number: 63-22327
 21. Private communication, T. Madsen, Ferroperm Quality Manager, 4th October, 2007
 22. Piezoelectric material parameters, Ferroperm website, www.ferroperm.com, September 2006
 23. Circuitworks Conductive Epoxy, CW2400, <http://www.chemtronics.com>, 2008
 24. N. Rajic, "A model for the piezoelectric transduction of stress waves," *Smart Mater. Struct.*, vol. 15, pp. 1151-1164 , 2006
 25. <http://www.fairchildsemi.com/pf/1N/1N5818.html>, 2008
 26. W. P. Mason, *Physical Acoustics Principles and Methods, Volume I - Part A*, pp.485-499 (Academic Press, New York and London, 1964), Library of Congress Catalog Card Number: 63-22327
 27. J. Johansson, P. Martinsson, "Incorporation of Diffraction Effects in Simulations of Ultrasonic Systems using Pspice models," *Proc. 2001 IEEE Ultrasonics Symposium*, vol. 1, pp. 405-410, Atlanta, GA, USA, 7-10 Oct. 2001
 28. G. S. Kino, *Acoustic Waves: Devices, Imaging and Analog Signal Processing*, Englewoods Cliffs, NJ: Prentice-Hall, 1988
 29. H. Seki, A. Granato, R. Truell, "Diffraction Effects in the Ultrasonic Field of a Piston Source and Their Importance in the Accurate Measurement of Attenuation," *The J. Acoust. Soc. Amer.*, vol. 28, no. 2, pp230-238, Mar. 1956

Appendix A: Example piezo parameter calculation

To calculate ϵ_{33}^S : given that the permittivity $\epsilon_{33}^T = \epsilon_{33,r}^T \epsilon_0$ van Deventer *et al* [15] gives the following relationship between ϵ_{33}^T and ϵ_{33}^S ,

$$\frac{\epsilon_{33}^T}{\epsilon_{33}^S} = \frac{1}{1 - (k_{33})^2} \quad (\text{A1})$$

Because k_{33} and ϵ_{33}^T are normally provided by the manufacturer, ϵ_{33}^S may be calculated using equation A1.

To calculate e_{33} : piezoelectric constant e_{33} may be calculated using,

$$e_{33} = 2d_{31} c_{13}^E + d_{33} c_{33}^E \quad (\text{A2})$$

Equation A2 can be used if the manufacturer specifies c_{13}^E and c_{33}^E . If these elastic stiffness's are not provided then e_{33} may be estimated using,

$$e_{33} = d_{33} Y_{33}^E \sqrt{1 - (k_T)^2} \quad (\text{A3})$$

Equations A2 and A3 can be used to calculate an accurate e_{33} for most types of PZT ceramic, however the calculated e_{33} can be erroneous for PZT with unusual microstructure (e.g. Pz21 and Pz46).

To calculate c_{33}^D : The relationship between c_{33}^D and c_{33}^E is,

$$\frac{c_{33}^D}{c_{33}^E} = \frac{1}{1 - (k_T)^2} \quad (\text{A4})$$

A PZT manufacturer normally specifies both k_T and c_{33}^E allowing c_{33}^D to be found. If the manufacturer does not specify c_{33}^E then it will need to be found from Y_{33}^E ,

$$c_{33}^E = \frac{Y_{33}^E}{1 - A^2} \quad (\text{A5})$$

Assuming that k_T , k_{33} , and k_P are known for a material, the constant A can be found from the relationship given by Berlincourt *et al* [20],

$$k_T = \frac{k_{33} - A k_P}{\sqrt{1 - A^2} \sqrt{1 - k_P^2}} \quad (\text{A6})$$

A can also be found from its definition,

$$A = \frac{\sqrt{2} s_{13}^E}{\sqrt{s_{33}^E (s_{11}^E + s_{12}^E)}} \quad (\text{A7})$$

where s_{13}^E , s_{33}^E , s_{11}^E and s_{12}^E are compliances at constant field.

With c_{33}^D known then v_D , the clamped speed of sound in the piezoelectric material, can be found using,

$$v_D = \sqrt{\frac{c_{33}^D}{\rho}} \quad (\text{A8})$$

Also required for lumped element modelling are the density and speed of sound of the medium that the PZT element is situated in. For the example shown in Figure 1a the surrounding medium is air, which has density $\rho = 1.25 \text{ kg/m}^3$ and speed of sound $v = 343.4 \text{ m/s}$. Knowing the area A_E of the PZT element allows the mechanical loading due to the medium to be found,

$$Z_0 = \rho v A_E \quad (\text{A9})$$

Using a single resistor Z_0 to model the medium is equivalent to making the assumption that no acoustic echo will be received back from the medium [16].

Appendix B: LTSpice netlists

Given below are example of LTSpice library and schematic files used to perform the modelling shown in this paper. Note that the parameters given in PZTtrans.lib are defined in Appendix C.

B.1. PZTtrans.lib

```
*PUTTMER 1997 THICKNESS-MODE TRANSDUCER
.SUBCKT PZTtrans E B F
O1 B 1 F 1 myLossyTlineTRANS
V1 1 2
E1 2 0 4 0 1
V2 E 3
C0 3 0 {c0T}
F1 0 3 V1 {hc0T}
F2 0 4 V2 {hT}
R1 4 0 1E3
C1 4 0 1
.model myLossyTlineTRANS LTRA(len={thickT} R={rT} L={LT} C={cT})
.ENDS
```

B.2. PZTtrans.asy

```
Version 4
SymbolType BLOCK
RECTANGLE Normal 48 48 -48 -48
TEXT -48 -1 Left 0 PZTtrans
SYMATTR Value PZTtrans
SYMATTR Prefix X
SYMATTR SpiceModel PZTtrans.lib
SYMATTR Value2 PZTtrans
PIN -48 -32 LEFT 8
PINATTR PinName E
PINATTR SpiceOrder 1
PIN -48 32 LEFT 8
PINATTR PinName B
PINATTR SpiceOrder 2
PIN 48 32 RIGHT 8
PINATTR PinName F
PINATTR SpiceOrder 3
```

B.3. const_power.lib

```

.subckt const_power in m_Power
B1 N001 0 V=V(vd)*sin(2*pi*time*V(f))
R1 in N001 50
*for real power the next line must be:
*B2 z1 0 V=-1*V(in)*i(r1)
*for apparent power the next line must be:
*B2 z1 0 V=abs(V(in)*i(r1))
B2 z1 0 V=abs(V(in)*i(r1))
R3 m_Power z1 1K
C2 m_Power 0 20n
V1 f 0 {fDRIVEcp}
V2 Gain 0 100
V3 Ideal_Power 0 {pDRIVEcp}
B4 0 vd I=V(Gain)*(V(Ideal_Power)-V(m_power))
R4 vd 0 1e8
C3 vd 0 10µ
.ic V(vd)=10
.ic V(m_power)={pGUESScp}
.backanno
.ends

```

Appendix C: Parameter values used in calculations

definition	designation	units	material				
			Hu PZT [9]	Pz27 [22]	aluminium [5]	steel [9]	silver epoxy [5]
Clamped relative permittivity	$\epsilon_{33,rel}^S$	-	1470.5	914	-	-	-
piezoelectric constant	e_{33}	C/m ²	23.3	16	-	-	-
clamped elastic modulus	c_{33}^D	GPa	159	144	73.1	269	7.28
density	ρ	kg/m ³	7500	7700	2770	7850	3890
mechanical quality	Q	-	136	81.5	1000	100	23.4

Definition	Designation	Equation	Effective Units
permittivity of free space	e0	8.8542×10^{-12}	C/(V.m)
clamped permittivity	eST	$e_{33}^S \cdot e_0$	C/(V.m)
piezoelectric constant	e33T		C/m ²
clamped elastic modulus	c33DT		N/m ²
density	rhoT		kg/m ³
mechanical Q	QT		-
disk thickness, and radius	thickT, radT		m
clamped velocity of sound	vDT	$\sqrt{c_{33}^D / \rho_T}$	m/s
anti-resonant frequency	resfreqT	$v_{DT} / (2 \cdot \text{thickT})$	Hz
disk area	areaT	$\pi \cdot \text{radT}^2$	m ²
capacitance	c0T	$e_{ST} \cdot \text{areaT} / \text{thickT}$	F
transmitting constant	hT hc0T	e_{33}^T / e_{ST} $h_T \cdot c_{0T}$	V/m F.V/m
acoustic impedance*area	z0T	$\rho_T \cdot v_{DT} \cdot \text{areaT}$	kg/s
lossy transmission line inductance	LT	z_{0T} / v_{DT}	kg/m
lossy transmission line capacitance	cT	$1 / (v_{DT} \cdot z_{0T})$	s/kg
lossy transmission line resistance	rT	$2 \cdot \pi \cdot \text{resfreqT} \cdot L_T / Q_T$	kg/(m.s)
density of medium back face	rhoTB		kg/m ³
velocity of sound in back medium	vDTB		m/s
acoustic impedance*area	z0TB	$\rho_{TB} \cdot v_{TB} \cdot \text{areaT}$	kg/s
density of medium front face	rhoRB		kg/m ³
velocity of sound in front medium	vDRB		m/s
acoustic impedance*area	z0RB	$\rho_{RB} \cdot v_{RB} \cdot \text{areaT}$	kg/s

DEFENCE SCIENCE AND TECHNOLOGY ORGANISATION DOCUMENT CONTROL DATA				1. PRIVACY MARKING/CAVEAT (OF DOCUMENT)	
2. TITLE Modelling and Experimental Validation of the Acoustic Electric Feedthrough Technique			3. SECURITY CLASSIFICATION (FOR UNCLASSIFIED REPORTS THAT ARE LIMITED RELEASE USE (L) NEXT TO DOCUMENT CLASSIFICATION) Document (U) Title (U) Abstract (U)		
4. AUTHOR(S) Scott Moss, Phillip McMahon*, Michael Konak, Chris Phoumsavanh, Nik Rajic, Steve Galea, Ian Powlesland			5. CORPORATE AUTHOR DSTO Defence Science and Technology Organisation 506 Lorimer St Fishermans Bend Victoria 3207 Australia		
6a. DSTO NUMBER DSTO-RR-0338		6b. AR NUMBER AR-014-343		6c. TYPE OF REPORT Technical Report	
				7. DOCUMENT DATE November 2008	
8. FILE NUMBER 2007/1098511/1	9. TASK NUMBER LLR 07/250	10. TASK SPONSOR CAVD	11. NO. OF PAGES 32		12. NO. OF REFERENCES 29
13. URL on the World Wide Web http://www.dsto.defence.gov.au/corporate/reports/DSTO-RR-0338.pdf			14. RELEASE AUTHORITY Chief, Air Vehicles Division		
15. SECONDARY RELEASE STATEMENT OF THIS DOCUMENT <i>Approved for public release</i>					
OVERSEAS ENQUIRIES OUTSIDE STATED LIMITATIONS SHOULD BE REFERRED THROUGH DOCUMENT EXCHANGE, PO BOX 1500, EDINBURGH, SA 5111					
16. DELIBERATE ANNOUNCEMENT No Limitations					
17. CITATION IN OTHER DOCUMENTS Yes					
18. DSTO RESEARCH LIBRARY THESAURUS http://web-vic.dsto.defence.gov.au/workareas/library/resources/dsto_thesaurus.shtml Smart structures, Smart materials, Piezoelectric materials, Power engineering, Communications engineering					
19. ABSTRACT This report outlines an investigation of an ultrasonic Acoustic Electric Feedthrough (AEF) to transfer power through a metal plate. This approach is being explored as a potential means of wirelessly powering in situ structural health monitoring systems embedded within aircraft and other high value engineering assets. A numerical model is developed describing the coupled electro-mechanical behaviour of an AEF system, and is then validated using experimental data. Using a pair of well matched piezoelectric disks with 38 mm diameter and 2 mm thickness, and with 1 W of real input power, the AEF approach is shown to transfer approximately 300 mW of usable electrical power through aluminium plate with thicknesses in the range of 1.6 mm - 5 mm.					